

Koopman spectral analysis of separated flow over a finite-thickness flat plate with elliptical leading edge

Jonathan H. Tu^{*}; Clarence W. Rowley[†]

Princeton University, Princeton, NJ 08544

Ehsan Aram[‡]; Rajat Mittal[§]

Johns Hopkins University, Baltimore, MD 21218

The separated flow over an airfoil is characterized by up to three distinct natural frequencies: those of the shear layer, separation bubble, and wake. Previous work has shown that open-loop forcing at sub- and super- harmonics of these frequencies can be especially effective in controlling the extent of the separation bubble. Unfortunately, an understanding of the mechanisms driving this behavior is far from complete. In this work, we investigate the interactions between the shear layer and wake using a combination of direct numerical simulations and spectral analysis. We simulate the forced and unforced flows over a finite-thickness flat plate using an immersed boundary method. Spectral analysis of the resulting dynamics is performed using the Koopman operator, a linear operator applicable even to nonlinear systems, as well as traditional signal processing techniques. Using these two approaches, we identify pertinent flow structures based on their frequency content and posit the nature of their interactions.

Nomenclature

U_∞	freestream velocity, defined at upstream boundary of domain
t	thickness of flat plate
c	chord length of flat plate
x/c	distance from leading edge, measured in chord lengths
\bar{v}_j	average velocity of synthetic jet during expulsion phase
d_j	width of synthetic jet slot
$C_\mu = \bar{v}_j^2 d_j / U_\infty^2 c$	momentum coefficient for synthetic jet
$F^+ = fc / U_\infty$	nondimensional frequency
d_w	width of wake
$St = fd_w / U_\infty$	Strouhal number
PSD	power spectral density

I. Introduction

A. Overview

With ever-increasing demands for improved performance and increased efficiency, the control of separated flows has drawn considerable attention. In this work, we are concerned with the flow over an airfoil, wherein

^{*}Graduate Student, Mechanical and Aerospace Engineering, Student Member, AIAA.

[†]Associate Professor, Mechanical and Aerospace Engineering, Associate Fellow, AIAA.

[‡]Graduate Student, Mechanical Engineering, Student Member, AIAA.

[§]Professor, Mechanical Engineering, Associate Fellow, AIAA.

decreased separation can improve the lift-to-drag ratio.¹ Such flows display highly complex behavior, characterized by shear layer instability and vortex shedding in the wake, and in some cases periodic shedding of the separation bubble. In spite of this, much progress has been made in controlling separation, for instance by implementing zero-net-mass-flux (ZNMF) actuators. These devices, also known as synthetic jets, are favored due to their relatively simple design. Furthermore, the periodic excitation they produce has been shown to be more effective than steady forcing.²

ZNMF actuators are also versatile, in that the forcing frequency can be adjusted to suit a particular flow. Much research effort has been focused on finding an optimal operating frequency, but as of yet there is no consensus. The variation in reported values indicates a need for an increased appreciation of the rich, nonlinear dynamics driving these flows. For instance, the forcing frequency is often nondimensionalized with respect to the shedding frequency of the separation bubble, without considering the wake frequency or any interactions therein.³

In fact, separated airfoil flows are characterized by up to three distinct frequencies, associated with the shear layer, separation bubble, and wake.³ In this work, we will investigate the interactions between the shear layer and wake for an open separation bubble. We consider a *canonical separated flow*, in which separation is induced over a finite-thickness flat plate at zero angle-of-attack by a blowing and suction boundary condition. Using two-dimensional (2-D) direct numerical simulations, we find the dominant natural frequencies of the flow with and without ZNMF actuation. (Preliminary simulations show that 3-D effects are confined to the downstream wake. While these are certainly important, the interactions in which we are interested are observed in and believed to drive the 2-D flow as well.) We then perform a spectral analysis using both traditional signal processing techniques as well as the Koopman operator, identifying relevant flow structures based on their frequency content. The nature of these structures provides insight into the interactions between the shear layer and wake.

The following sections discuss in more detail previous studies concerning ZNMF actuation of separated airfoil flows. In Section B, we summarize recent work regarding optimal forcing frequencies and the lack of consensus among reported values. In Section C we present work suggesting that the rich dynamics of the separated airfoil flow can be utilized for flow control purposes. Specifically, a number of *lock-on states* exist, some of which display desirable lift and drag characteristics.

B. Difficulties in finding an optimal forcing frequency

Much of the research related to ZNMF actuation is concerned with finding an optimal open-loop forcing frequency. A nondimensional frequency, F^+ , can be defined using length and velocity scales associated with some natural frequency in the flow. (The velocity scale is often taken to be U_∞ , the freestream velocity.) For studies where the length is scaled by the chord length c , a range of values $0.55 < F^+ < 5.5$ has been reported to be optimal (Bar-Sever,⁴ Seifert *et al.*,⁵ Ravindran,⁶ Wygnanski,⁷ Margalit,⁸ Darabi & Wygnanski,⁹ Funk & Parekh¹⁰). For the length scales X_{TE} (distance from the actuator to the trailing edge) and L_{sep} (length of the separation bubble), optimal ranges of $0.50 < F^+ < 2.0$ (Seifert & Pack,¹¹ Greenblatt & Wygnanski,¹² Pack *et al.*¹³) and $0.75 < F^+ < 2.5$ (Seifert *et al.*,² Pack & Seifert,¹⁴ Gilarranz & Rediniotis¹⁵) have been reported, respectively. As an extreme example, Amitay *et al.*¹⁶ found that for an unconventional airfoil, forcing at $F^+ > 10$ outperformed configurations with $F^+ < 4$. The magnitude of these discrepancies may seem insignificant, but Seifert *et al.*⁵ reported a corresponding 25% change in the lift coefficient C_L when F^+ was varied between 0.25 and 1.5. Similarly, Wygnanski⁷ found a 400% increase in the momentum coefficient C_μ for the same range of F^+ .

Even taking into account the varying definitions of F^+ , it is clear that there is no consensus on its optimal value. This is not a complete surprise, given the highly complex behavior of these flows. For instance, in a separated airfoil flow where the mean separation bubble remains detached, there are two dominant frequencies: those of the shear layer and wake. This is typical of a bluff body flow, and studies in this field typically focus on the latter frequency and not the former.¹⁷⁻¹⁹ Only Wu *et al.*²⁰ consider both parameters. When the mean flow reattaches, there can be a third natural frequency, associated with the shedding of the separation bubble. The lack of agreement on an optimal F^+ value may indicate a need to consider all of these frequencies, as well any coupling between them. For a nice overview of these issues, see Mittal *et al.*³

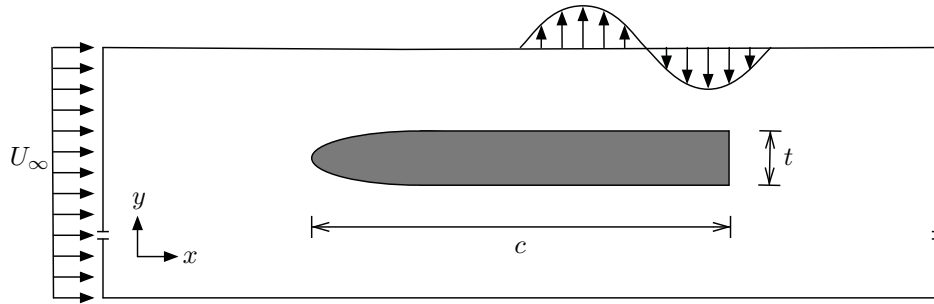


Figure 1. Schematic of the canonical separated flow. A finite-thickness flat plate with an elliptical leading edge is subjected to uniform incoming flow. A separation bubble is induced by a steady blowing/suction boundary condition applied along the upper boundary of the computational domain.

C. Exploiting lock-on states for flow control

Though separated airfoil flows are characterized by up-to three natural frequencies, in certain flow configurations some of these may take on the same value. We refer to such states as *lock-on states*. Kotapati *et al.*²¹ simulated a configuration in which the unforced flow locked onto a single frequency. That is, the shear layer, separation bubble, and wake frequencies were equal. For this system, actuation at the natural frequency or its first subharmonic resulted in a coupling of the separation bubble frequency with a superharmonic of the forcing frequency. On the other hand, forcing at superharmonics caused the wake and separation bubble to lock onto a subharmonic of the forcing frequency. It was observed that forcing at the first superharmonic significantly improved the lift-to-drag ratio, while forcing at further superharmonics was detrimental. Given the rich system dynamics, it is likely that more of these lock-on states exist, some of which may have desirable lift and/or drag properties. By increasing our understanding of the complex interactions between the shear layer, separation bubble, and wake, we may improve our ability to exploit these states for control purposes.

II. Flow Configuration

A. The canonical separated flow

All simulations are performed using a *canonical separated flow*. In this configuration, a finite-thickness flat plate with an elliptical leading edge is placed in a uniform oncoming flow at zero angle-of-attack. A separation bubble is induced through a steady blowing/suction boundary condition applied at the top of the computational domain (Figure 1). By using a flat plate geometry, we eliminate the influence of curvature, which has been shown to significantly affect the nature of the boundary layer,²² as well as the receptivity of the flow to actuation.^{23,24} Furthermore, by varying the location of the plate and the amplitude of the blowing/suction boundary condition, we can specify both the location and extent of the separation bubble, something not possible by setting the angle-of-attack and freestream velocity alone.³

B. Geometry

In this study, we consider a flat plate with a 4:1 elliptical leading edge and a thickness-to-chord ratio $t/c = 0.095$. The upper surface of the flat plate is placed $0.15c$ from the upper wall, with the leading edge $0.5c$ downstream of the uniform inflow. The inflow (freestream) velocity is chosen such that $Re_c = 100,000$. This is similar to the experimental setup analyzed by Aram *et al.*²⁵

We analyze three particular implementations of the blowing/suction boundary condition. First, we consider an attached flow, for which there is no blowing/suction at the upper wall; instead, we apply a no-slip boundary condition. To physically separate the shear layer from the wake, we also consider a configuration in which separation is imposed near the midchord. Specifically, the vertical velocity v is varied in a region spanning $x/c = 0.45$ to $x/c = 0.95$. Finally, we consider a configuration where separation is imposed closer to the trailing edge, with blowing/suction enforced from $x/c = 0.75$ to $x/c = 1.25$. In both cases, the vertical velocity in the blowing/suction region varies sinusoidally in the streamwise direction, with an amplitude of

$0.65U_\infty$. (The boundary conditions do not vary with time.)

C. Actuation

We also study the effect of ZNMF forcing, placing a synthetic jet on the upper-surface at $x/c = 0.6$. We use a “slot-only” model for jet, with a slot width and depth of $0.01c$.²⁶ The jet generates a uniform vertical velocity across the bottom of the slot. (In this model the jet cavity is not modeled at all.) The slot velocity varies sinusoidally in time, with an amplitude such that the mean jet velocity (during expulsion) is $\bar{v}_j = 0.15U_\infty$. This results in a momentum coefficient $C_\mu = 2.25 \times 10^{-4}$. For this study we force the flow at $F^+ = 2.2$. (From here on out, we use the definition $F^+ = fc/U_\infty$.)

III. Numerical Methods

A. Direct numerical simulation

We perform 2-D simulations using an immersed boundary code. The Navier-Stokes equation is discretized using a cell-centered, collocated arrangement of the primitive variables. A second-order Adams-Bashforth scheme is used for the convective terms, and an implicit Crank-Nicolson scheme for the diffusive terms. To advance in time, we employ a second-order fractional-step method. This code has been validated extensively by comparisons with published numerical and experimental data.^{27,28}

The simulations are run on a domain with dimensions $2c \times 0.76c$ (in x and y). The grid resolution is 512×256 , with a nonuniform spacing. At the upper surface, a no-slip boundary condition is enforced, except in the blowing/suction region, where the vertical velocity varies sinusoidally (in space), with an amplitude of $0.65U_\infty$. The horizontal velocity is subjected to an outflow boundary condition in this region. Downstream, we also implement an outflow boundary condition. At the lower surface, we enforce a no-slip boundary condition. This setup is designed to match an existing experimental configuration, similar to that analyzed by Aram *et al.*²⁵

B. Koopman analysis

The Koopman operator is an infinite-dimensional, linear operator that can be used to perform spectral analysis of nonlinear dynamical systems, as suggested by Rowley *et al.*²⁹ in the context of fluid mechanics. Suppose we have a discrete-time dynamical system where $x_{k+1} = f(x_k)$. For instance, x_k could be the state of a flow at one instant in time, and x_{k+1} the state some time Δt later. Let $g(x_k)$ be a scalar-valued function. g could give the spanwise vorticity at a single point in the flow, say. Then the Koopman operator U maps g to a new function Ug , such that

$$Ug(x_k) = g(f(x_k)) = g(x_{k+1}). \quad (1)$$

We note that though f may be a nonlinear map, U acts linearly on functions g .

If we let λ_j and ϕ_j be the eigenvalues and eigenfunctions of U , then a vector-valued function \mathbf{g} , called an *observable*, can be decomposed as

$$\mathbf{g}(x_k) = \sum_{j=1}^{\infty} \lambda_j^k \phi_j(x_0) \mathbf{v}_j, \quad (2)$$

where we refer to the \mathbf{v}_j as *Koopman modes*. (An example of an observable would be a vector describing the spanwise vorticity at a finite number of points in the flow.)

Each Koopman mode \mathbf{v}_j is associated with a single eigenvalue λ_j , and consequently a single frequency. If \mathbf{g} is a vector of measurements made at each gridpoint in a simulation, then the Koopman modes are spatial structures. Thus using Koopman analysis, we can identify flow structures based on their frequency content. For systems that are characterized by their frequencies, the Koopman operator is a natural tool to apply.

In general, it is unclear how one would compute Koopman modes. For fluid flows, we can approximate them using an Arnoldi-like algorithm sometimes called dynamic mode decomposition (DMD).^{29,30} DMD is a snapshot based method, similar to proper orthogonal decomposition (POD). Suppose we take snapshots from a simulation, sampled regularly in time. Then given a set of snapshots $\{\hat{\mathbf{x}}_j\}_{j=0}^n$, the DMD algorithm

generates eigenvalues $\{\widehat{\lambda}_j\}_{j=1}^n$ and eigenmodes $\{\widehat{\mathbf{v}}_j\}_{j=1}^n$ such that

$$\begin{aligned}\widehat{\mathbf{x}}_k &= \sum_{j=1}^n \widehat{\lambda}_j^k \widehat{\mathbf{v}}_j & k = 0, \dots, n-1 \\ \widehat{\mathbf{x}}_n &= \sum_{j=1}^n \widehat{\lambda}_j^n \widehat{\mathbf{v}}_j + \mathbf{r} & \mathbf{r} \perp \text{span}\{x_k\}_{k=0}^{n-1}.\end{aligned}\tag{3}$$

We see that for the first n snapshots, we can exactly reproduce $\widehat{\mathbf{x}}_k$ using the DMD eigenmodes and eigenvalues. For the last snapshot, there is a small residual if the same reconstruction equation is applied. The DMD modes are the modes that minimize this residual, in a least-squares sense.^{29, 30}

The DMD decomposition is nearly identical to the Koopman decomposition (see Equation (2)) if we take

$$\begin{aligned}x_k &= \widehat{\mathbf{x}}_k \\ \mathbf{g}(x_k) &= x_k \\ \widehat{\mathbf{v}}_j &= \phi(x_0) \mathbf{v}_j.\end{aligned}$$

The key difference is that the sums in (3) are finite, while those in (2) are infinite. That allows the Koopman decomposition to reproduce trajectories of \mathbf{g} that may be nonlinear, whereas the the DMD decomposition can at best reproduce linear dynamics.

Since the DMD modes exactly reproduce the first n snapshots using these linear dynamics, we interpret them as the eigenmodes of a linear system that approximates the true, nonlinear system in a small neighborhood. In other words, if the true Navier-Stokes equations can be described by a map $\widehat{\mathbf{x}}_{k+1} = \mathbf{f}(\widehat{\mathbf{x}}_k)$, the DMD modes are eigenmodes of an approximating linear system $\widetilde{\mathbf{x}}_{k+1} = \mathbf{A}\widetilde{\mathbf{x}}_k$, where $\widetilde{\mathbf{x}}_k = \widehat{\mathbf{x}}_k$ for $k = 0, \dots, n-1$. At the n^{th} iteration, the linear map no longer matches the nonlinear one, as seen in (3). Because the Koopman modes of a linear system are simply its eigenmodes,²⁹ the DMD modes give us an approximation of the Koopman modes for the nonlinear system. For clarity, we will now drop the ‘‘hat’’ notation for DMD modes, assuming that they are in effect equal to Koopman modes (modulo scaling by $\phi(x_0)$).

IV. Results

A. Unforced flow

1. Power spectrum analysis

When no separation is induced, we simply have flow past a bluff body, and indeed, we observe the familiar von Kármán vortex street (Figure 2). Measuring v with a probe placed in the wake, we find that the resulting power spectrum shows a dominant peak at $F^+ = 3.00$ (Figure 3). We also see secondary and tertiary peaks near the second and first superharmonics of the wake frequency, at $F^+ = 9.33$ and $F^+ = 6.33$.

In the case of midchord separation, the shear layer detaches around $x/c = 0.4$ and rolls up into distinct vortices around $x/c = 0.6$ (Figure 2). These vortices convect downstream but are pushed downward toward the flat plate by the blowing boundary condition along the upper wall. The shear layer reattaches and the wake is similar to that of the attached flow.

For this case, the power spectrum from the wake probe has a dominant peak at $F^+ = 3.0$, a secondary peak at $F^+ = 8.67$, and a weak tertiary peak at $F^+ = 5.67$ (Figure 3). As with the attached flow, these are roughly harmonics of the fundamental wake frequency. We note that the first superharmonic appears much more clearly in the data from a probe placed in the shear layer, which has a spectral peak at $F^+ = 5.67$. It appears that in this configuration, the shear layer frequency locks onto the first superharmonic of the wake frequency.

When the separation point is moved near the trailing edge, the shear layer no longer reattaches and the wake structure is highly complex (Figure 2). Using a probe placed in the wake, we can again identify a dominant wake frequency, at $F^+ = 2.33$, but the spectrum has no clear secondary or tertiary peak. (Somewhat isolated peaks are visible at $F^+ = 9.00$ and $F^+ = 6.67$, but these are of relatively low amplitude.) Data taken from a shear layer probe generates a messier spectrum, with the biggest peak near the second superharmonic of the wake frequency, at $F^+ = 6.67$. This peak is of lower amplitude than was seen for the

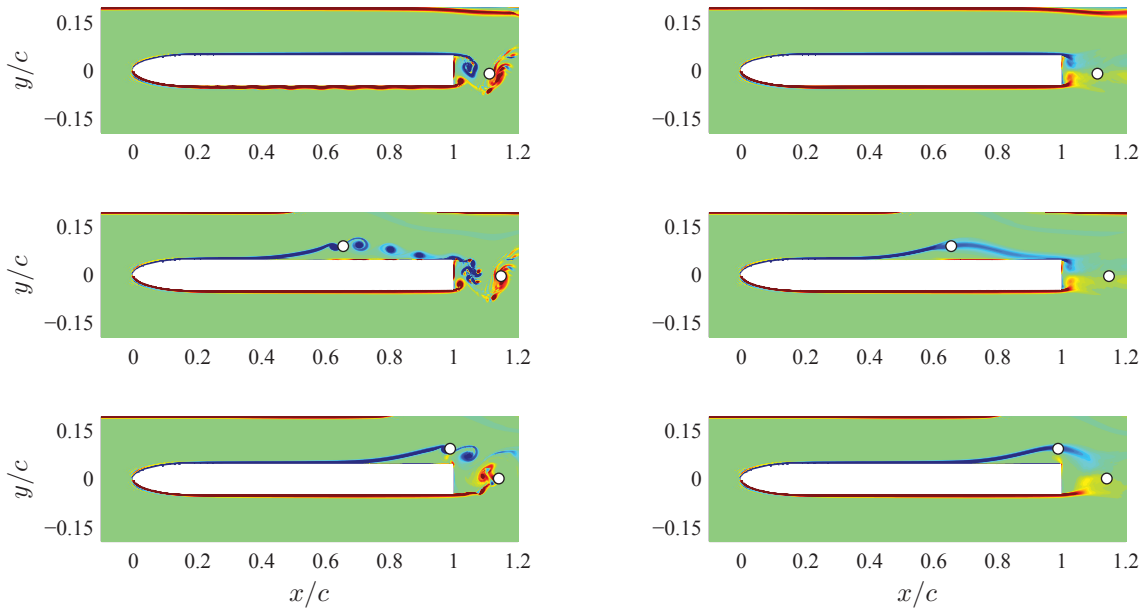


Figure 2. Instantaneous (left) and time-averaged (right) vorticity fields of the unforced flow. Three cases are considered: no separation (top), midchord separation (middle), and trailing edge separation (bottom). Probe locations are denoted by (o). As the separation point is moved aft, the shear layer no longer reattaches, and the wake structure becomes more complex.

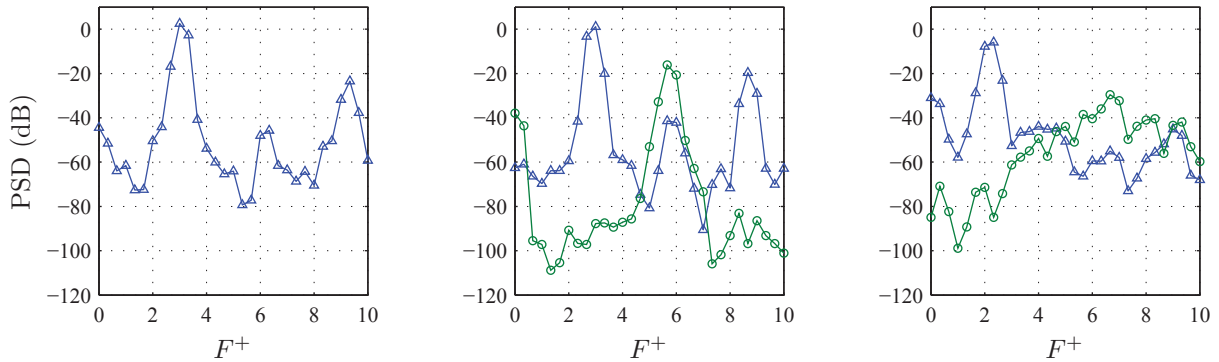


Figure 3. Power spectra for the unforced flow when no separation is induced (left), when separation is induced at the midchord (middle), and when separation is induced at the trailing edge (right). The spectra are computed from measurements of v taken in the wake (blue triangles) and in the shear layer (green circles). In all three cases, a dominant wake frequency is easily identified. For midchord separation, the shear layer frequency is also clear, while for trailing edge separation, the peak in the shear layer spectrum is less isolated.

shear layer in the case of midchord separation, and is not nearly as sharp nor isolated. As such, from the probe data alone, it is difficult to determine whether or not this is the characteristic shear layer frequency.

2. Frequency scales

The flows considered above represent three fundamentally distinct types of separated flows, namely those with no separation bubble (attached flow), a closed separation bubble, and an open separation bubble. In each case, a dominant wake frequency can be identified from probe data collected in the wake region. This suggests that for these flow configurations, the wake is the dominant flow structure. As such, it is logical to scale frequencies not by chord length, but by wake width.

We define the upper boundary of the wake as the point above the trailing edge where the horizontal

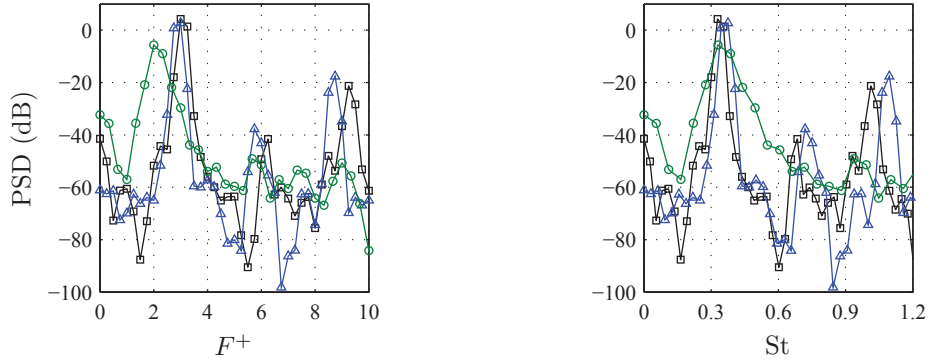


Figure 4. Comparison of frequency scalings for power spectra computed from measurements of v taken by wake probes. Spectra for the attached (black squares), midchord separation (blue triangles), and aftchord separation (green circles) cases are shown. We see that the dominant wake frequencies agree when the frequency is scaled by the wake width (right) instead of the chord length (left).

velocity u first reaches 99% of the maximum value it attains above the plate. We choose this definition because unlike a standard boundary layer where the velocity asymptotically approaches the freestream value, in this configuration, the constriction of the flow between the upper wall and the flat plate causes a net acceleration. Furthermore, the amount of acceleration varies based on the extent of the separation bubble. Thus there is no single velocity scale that can be applied in all cases, and the local maximum value was chosen instead. The lower wake boundary is defined similarly, but with respect to maximum velocity achieved below the plate. We must consider the two boundaries separately due to the asymmetry of the flow configuration.

With this scaling, we see that the wake frequencies agree (Figure 4). This is in contrast to the trend in F^+ , where there seemed to be a clear decrease in the wake frequency for trailing edge separation. (We do note, however, that for this case there is a significantly wider peak in the spectrum.) The agreement in wake frequency is not surprising, as Strouhal number is the natural parameter for characterizing a bluff body flow. Because it provides a common reference point for comparing frequencies across flow configurations, we use St in place of F^+ for the remainder of this analysis.

3. Limitations of probe data

One drawback of relying on probes for analysis is that the data can be sensitive to the probe locations. To demonstrate this, we consider the unforced flow with separation at the trailing edge. We compare our original probe, located in the shear layer at $(x/c, y/c) = (0.99, 0.09)$, to one placed slightly upstream, at $(x/c, y/c) = (0.94, 0.10)$. Both resulting spectra have their largest peak at $St = 1.10$ (Figure 5). However, this peak is almost 25 dB smaller for the upstream probe, and the shapes of the peaks are dissimilar. Furthermore, the upstream probe has a clear secondary peak at the wake frequency ($St = 0.33$), despite being located farther from the wake region. Without further analysis, it is unclear whether this indicates a secondary frequency in the shear layer, or that the probe is simply picking up frequencies from the wake oscillation.

To account for the sensitivity to location, we can simply add more probes, hoping to see clear trends that appear for many probe points. This can be done in computations at little cost, but is certainly not feasible in experiments. It will not generally solve the problem of having multiple peaks in a spectrum either. To determine the physical cause of each peak, we require something other than spectral data, motivating the use of spatial/modal analysis techniques such as POD and Koopman analysis.

Another drawback to traditional spectral analysis is its uniform discretization of frequency space, with the maximum observable frequency set by the Nyquist criterion and the spacing determined by the number of samples. As a result, frequencies of interest can only be computed up to some predetermined precision. Once data have been collected, there is little freedom to alter this. This highlights another advantage of Koopman spectral analysis, wherein the computed frequencies are not predetermined in any way, separating

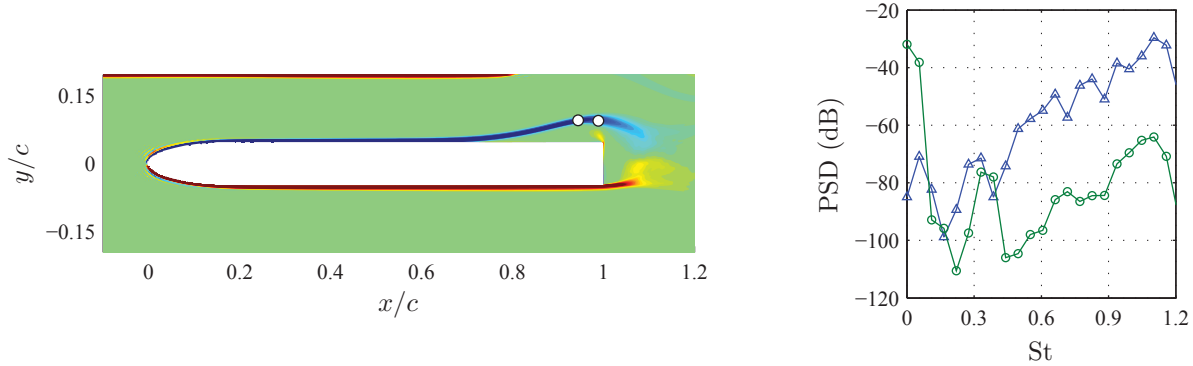


Figure 5. Time-averaged vorticity for the unforced flow with separation at the trailing edge (left), with two possible shear layer probes (\circ). The resulting spectra (right) share a peak at $St = 1.10$. However, the peaks for the upstream probe (green) are generally of much smaller amplitude than those for the downstream probe (blue). Also, the upstream probe shows an isolated peak near the wake frequency, at $St = 0.33$, while the downstream probe does not.

it from methods like the Discrete Fourier Transform (DFT).

4. Koopman analysis

As a complement to the traditional spectral analysis discussed above, we also compute Koopman modes using snapshots of the flow. In each computation, we take snapshots spanning 20,000 timesteps, sampled every 100 steps. (Each timestep is 0.002 convective time units.) For these flows, none of the Koopman eigenvalues are unstable, with most lying near the unit circle (neutrally stable). To clean up the spectra, we disregard any eigenvalues for which $\|\lambda\|^{50} < 2/3$. Recalling Equation (3), we see these correspond to modes whose contribution to a snapshot decreases by $1/3$ over 50 samples (one convective time unit).

The Koopman spectrum for the attached flow is shown in Figure 6. We see three clear peaks at the wake frequency ($St = 0.34$) and its first two superharmonics ($St = 0.68, 1.02$), matching the spectrum shown in Figure 3. The corresponding Koopman modes also show clear, spatially harmonic structures. For clarity, we discuss only structures in the v velocity field, noting that similar behavior is observed in u . The wake mode is characterized by large, up-down symmetric bubbles, alternating in sign in the streamwise direction (Figure 7, mode A). Its first superharmonic has a mode with antisymmetric pairs of bubbles, again alternating in sign as we move downstream (Figure 7, mode B). The second superharmonic mode is similar to the wake mode, but at a higher spatial frequency (Figure 7, mode C). These mode structures are characteristic of the flow past any bluff body, such as a 2-D cylinder.³¹

When separation is induced at the midchord, the behavior is very much the same. The Koopman spectrum shows three clear peaks at the wake frequency and its first two superharmonics ($St = 0.36, 0.72, 1.08$) (Figure 6). The corresponding Koopman modes show spatially harmonic wake structures, just as in the attached flow (Figure 7). However, there is also a clear shear layer structure in the $St = 0.72$ mode (Figure 7, mode E). This frequency is also observed in data taken from a shear layer probe (Figure 3), corroborating the conclusion that the shear layer is locking onto a superharmonic of the wake frequency.

For trailing edge separation, we get a fundamentally different Koopman spectrum. As before, we see a dominant peak at the wake frequency $St = 0.35$, as well as a secondary peak at its first superharmonic $St = 0.70$ (Figure 8). However, there is no secondary peak at the second superharmonic $St = 1.05$. Instead, there is a secondary peak at a slightly higher frequency of $St = 1.14$, and another secondary peak at $St = 1.50$. These nonharmonic peaks are not observed in the attached flow nor in the flow with midchord separation, and appear to be related to the increased complexity of the wake for the open separation bubble.

The wake mode has the same form as before, with symmetric bubbles of v now centered not at the middle of the flat plate, but at a slightly higher point (Figure 9, mode A). Looking at the bubble furthest upstream, we see that this wake structure seems to span the distance from the bottom of the flat plate to the upper boundary of the separation bubble (compare to Figure 2). Again, this motivates us to scale frequencies by

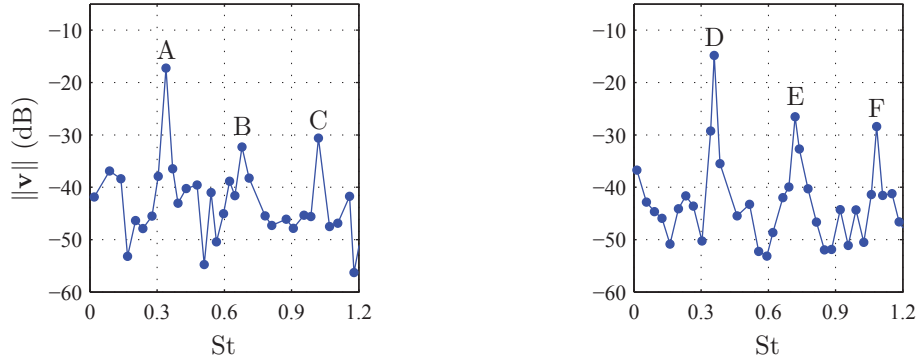


Figure 6. Koopman spectra for the unforced flow with no separation (left) and midchord separation (right). In both cases, clear peaks occur at the wake frequency and its first two harmonics.

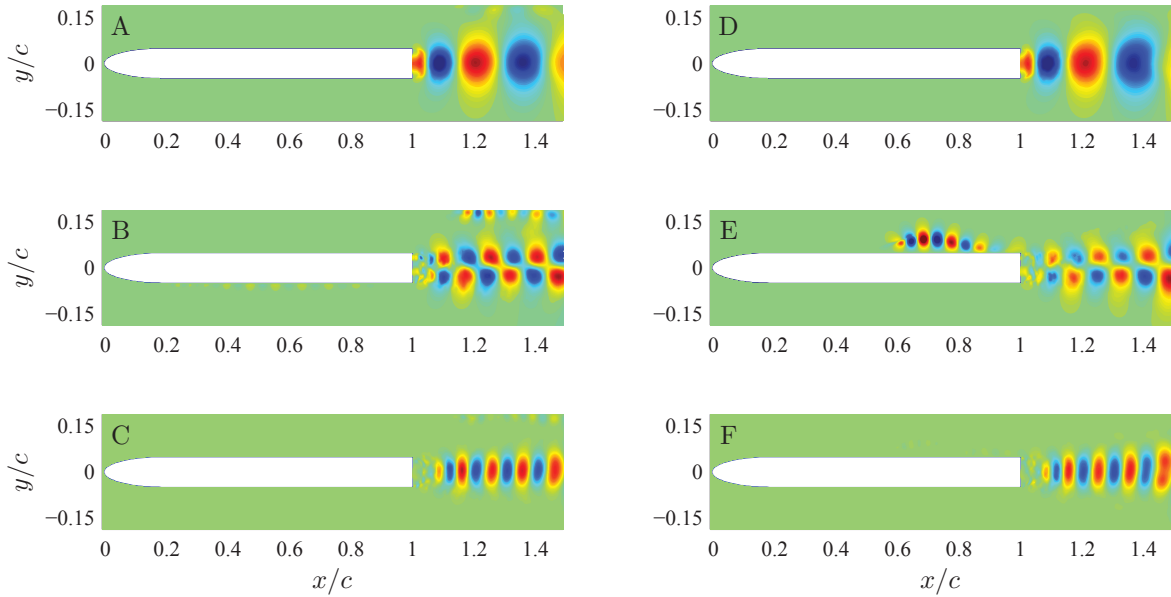


Figure 7. Comparison of Koopman modes for the unforced flow with no separation (left) and midchord separation (right). (Only contours of v are shown.) The three dominant modes occur at the wake frequency (top), its first superharmonic (middle), and its second superharmonic (bottom). (See Figure 6 for corresponding spectra.) The spatial structures are similar for both cases, with a slightly elongated wake in the case of midchord separation. For that case, it appears that the shear layer is locking onto the first superharmonic of the wake (middle, right).

wake width rather than chord length. The similarity of the wake mode in all three cases is consistent with the fact that the wake frequency is the same for all three.

We can also gain insight by comparing the Koopman modes to POD modes generated from the same data. POD modes identify spatial structures based on their energy content, while Koopman modes do so based on frequency content.²⁹ In addition, if computed from snapshots spanning a large time interval, the resulting POD modes are spatial structures that are uncorrelated in time (due to the orthogonality of the time coefficients). For the attached flow and flow with midchord separation, the Koopman modes and POD modes are nearly identical. Thus the modes corresponding to the wake and its superharmonics are also the highest energy structures in the flow, and are not correlated with each other. We might think of them as independent oscillators.

For the case of trailing edge separation, the wake mode appears as both a Koopman mode and a POD mode (Figure 9, modes A, A'). Again, we see that the wake is the dominant flow feature, with the most clearly

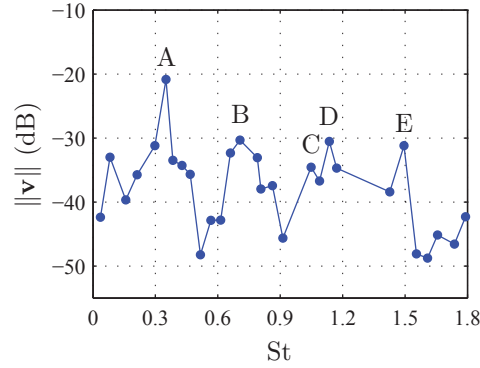


Figure 8. Koopman spectrum for the unforced flow with trailing edge separation. The wake frequency appears as the dominant peak (A), with its first superharmonic a secondary peak (B). There are also secondary peaks at nonharmonic frequencies (D, E). The peak corresponding to the second superharmonic (C) is weaker than the secondary peaks, unlike in the attached flow or the flow with midchord separation (see Figure 6).

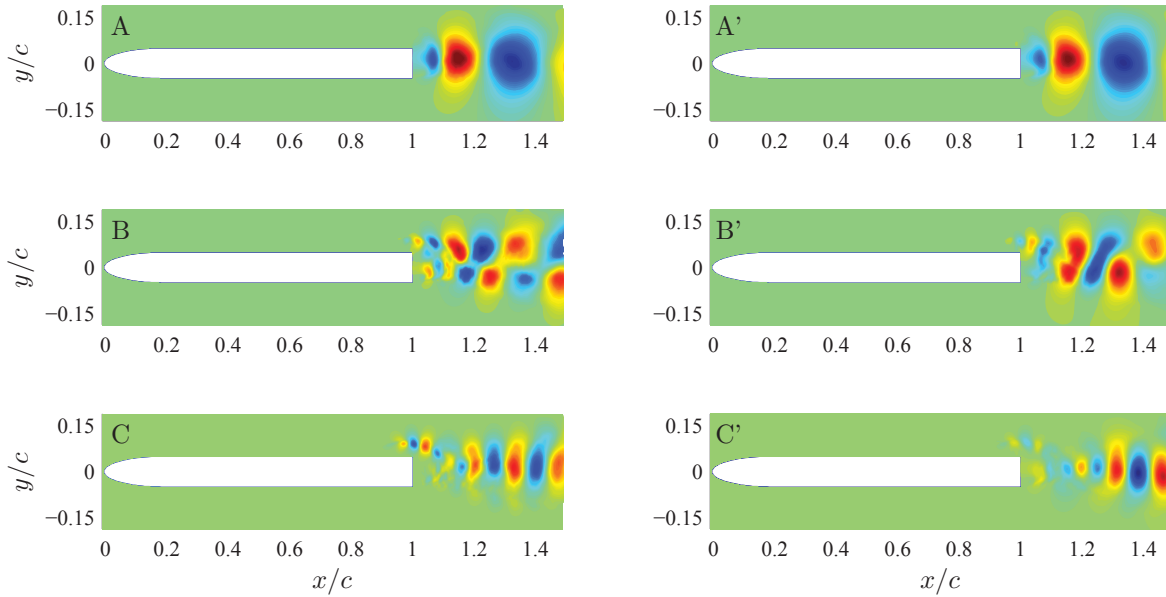


Figure 9. Comparison of Koopman modes (left) and POD modes (right) for the unforced flow with trailing edge separation. (Only contours of v are shown.) The dominant wake modes (top) are nearly identical. Only the Koopman modes show the expected spatially harmonic structures for the first (middle, left) and second (bottom, left) superharmonics. (See Figure 8 for corresponding spectrum.) The second (middle, right) and third (bottom, right) most energetic POD mode pairs show some evidence of these harmonics, but the structures are not nearly as clear.

identifiable frequency, as well as a high energy structure that is uncorrelated with any others. However, this is not the case with its superharmonics.

At the first superharmonic of the wake frequency, we see spatially harmonic structures similar to those observed in the attached flow and flow with midchord separation (Figure 9, mode B). The spatial structures again come in paired bubbles of v , but in this case they are not nearly as symmetric. The second most energetic POD mode pair is only slightly similar to this Koopman mode (Figure 9, mode B'). The lack of similarity suggests that this Koopman mode may be correlated with other structures in the flow.

These differences are even more apparent for the second superharmonic. Based on the Koopman spectrum, we don't expect this to be an important structure (Figure 8). The Koopman mode has a spatially

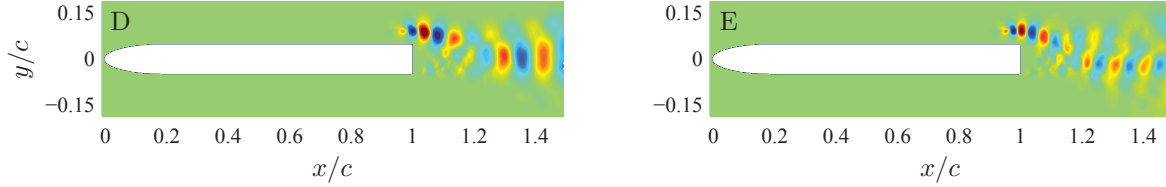


Figure 10. Koopman modes for the unforced flow with trailing edge separation. (Only contours of v are shown.) These two modes correspond to nonharmonic peaks in the spectrum (see Figure 8). Both exhibit strong support in the shear layer as well as the wake, and may be related to the interaction of the two structures.

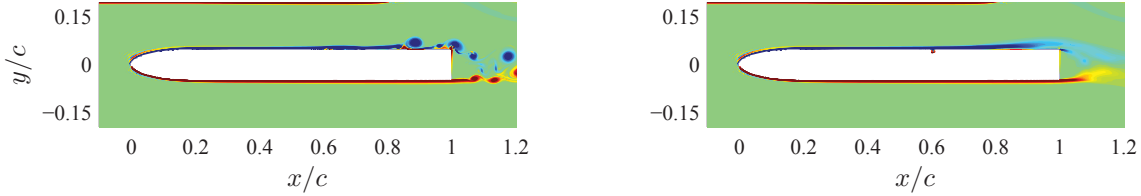


Figure 11. Instantaneous (left) and time-averaged (right) vorticity fields of the forced flow. A synthetic jet is placed on the upper surface at $x/c = 0.6$. ZNMF forcing at the wake frequency causes a drastic decrease in the extent of the separation bubble as compared to the unforced flow (see Figure 5).

harmonic structure as we would expect, but it bears only slight similarity to the third most energetic POD mode pair (Figure 9, modes C, C'), suggesting it is not a high energy structure. This is consistent with the relatively small peak in the Koopman spectrum. Again, the lack of similarity between the two modes also suggests that this Koopman mode may be correlated with other spatial structures.

This leads us to the nonharmonic peaks in the Koopman spectrum. The corresponding Koopman modes show strong support in the shear layer region as well as in the far wake (Figure 10). The presence of a shear layer structure in these modes is much stronger than in any other Koopman mode, suggesting that the nonharmonic modes may be fundamental to the behavior of the shear layer. In addition, the clear support in the downstream wake may indicate that these structures are responsible for the interaction between the shear layer and the wake. This is supported by the fact that neither interaction mode appears in POD analysis. As such, they may be correlated with other flow structures.

The frequency corresponding to the first interaction mode is $St = 1.14$, which is close to the frequency that was measured by shear layer probes ($St = 1.10$). This agreement suggests that this interaction mode may be the dominant shear layer structure, and that $St = 1.14$ is the characteristic shear layer frequency.

B. Actuated flow

Motivated by the dominance of the wake mode, we investigate the effect of actuating the flow with a synthetic jet oscillating at the wake frequency. We implement the actuator in the case of trailing edge separation, where the effect of separation is the greatest. With actuation, the shear layer still rolls up into distinct vortices, but these vortices convect downstream along the upper surface of the flat plate, with minimal separation (Figure 11). This results in a drastic reduction in the extent of the mean separation bubble, decreasing the height at the trailing edge from $0.062c$ to $0.037c$, a 40% change.

Koopman analysis shows that as a result of actuation, the dominant frequencies are again harmonics of the wake frequency (Figure 12). The nonharmonic peaks associated with the interaction modes no longer appear. The wake mode shows a similar structure to that of the unactuated flow, but the symmetry is broken by the effect of actuation (Figure 13, mode A). We see that the structures in the wake no longer extend above the upper surface of the flat plate. We also see evidence of actuation in the shear layer along the upper surface. In the unactuated flow, the wake mode showed no support in the shear layer.

The secondary peak in the Koopman spectrum occurs at the first superharmonic of the wake frequency (Figure 12). For each of the unactuated flows, this frequency corresponds to a spatially harmonic structure

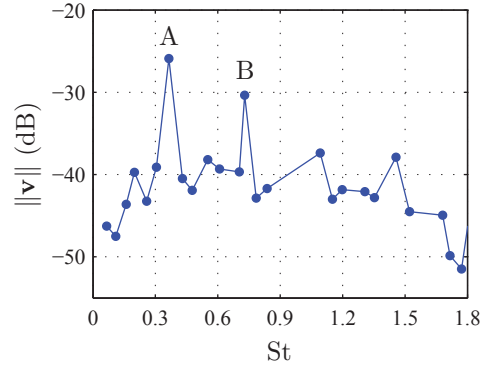


Figure 12. Koopman spectrum for the actuated flow with trailing edge separation. There are clear peaks at the wake/forcing frequency and its superharmonics. Unlike in the unforced flow, there are no peaks at nonharmonic frequencies (see Figure 8).

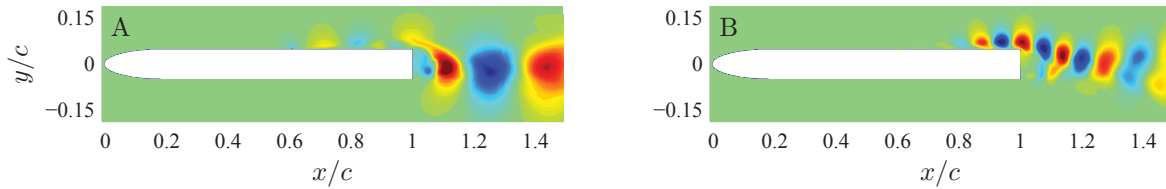


Figure 13. Dominant Koopman modes for the actuated flow with trailing edge separation. (Only contours of v are shown.) Forcing at the wake frequency decreases the size of the structures in the wake mode (left). It also causes the first harmonic mode to take a form more similar to the interaction modes (Figure 10) than the unforced superharmonic mode (Figure 9). (See Figure 12 for corresponding spectrum.)

characterized by antisymmetric pairs of bubbles in v , spanning the length of the wake. In contrast, for the actuated flow we observe the same superharmonic frequency, but no such harmonic structures. Instead, we see strong support in the shear layer, with structures that extend into the wake (Figure 13, mode B).

If anything, these structures are more similar to those of the interaction modes than anything else. All show clear support in the shear layer, with bubbles of v alternating in sign. These structures then extend downward into the wake. For the interaction modes, the far field wake structure is similar to that of the second wake superharmonic (Figure 10, mode D, Figure 9, mode C). However, for the actuated flow, the far field structures seem to be splitting, possibly into the harmonic structures expected for the first wake superharmonic. The second most energetic POD mode pair has the same structure, meaning this is a high energy mode that is uncorrelated with others.

Actuation appears to cause the first interaction mode to lock onto the first superharmonic of the wake, similar to the case of midchord separation. For midchord separation, there are two distinct regions of support in the first superharmonic mode, one in the shear layer and one in the wake (Figure 7). In the actuated flow with trailing edge separation, we instead see a combination of these structures, with one flowing into the other. This is in contrast to the unactuated flow, where the first interaction mode occurs at a nonharmonic frequency and has support in the shear layer and far wake, but not the near wake.

We recall that in the unactuated flow, the first interaction mode appears as a Koopman mode but not as a POD mode. This suggests that it could be correlated with other structures. In the actuated case, the Koopman and POD modes match, and are thus not coupled to other structures. As such, we might infer that the reason this particular choice of actuation is effective is that it enhances the interaction mode, such that the vortices from the shear layer can interact with the wake constructively and in an uncoupled manner, decreasing the extent of the wake.

V. Conclusions

Koopman analysis proves to be an effective complement to traditional spectral analysis. Using global data (snapshots of the velocity field) we are able to identify the dominant wake and shear layer frequencies, matching them to modes with corresponding spatial structures. This is especially useful when probe data produce spectra with multiple peaks, whose sources can be ambiguous. It also avoids the sensitivity of probe data to the location of the probe itself.

We analyze three unforced flows, with no separation, separation at the midchord, and separation at the trailing edge. When normalized by the wake width, the wake frequencies agree within 10%. This provides a common reference point for comparing flow frequencies. In the case of attached flow, the Koopman spectrum has peaks at the wake frequency and its superharmonics. For midchord separation, the same peaks are observed, with the shear layer locking onto the first superharmonic of the wake frequency.

When the separation point is moved near the trailing edge, the spectrum becomes more complex. The second superharmonic is no longer a dominant peak, and two nonharmonic peaks appear. The two corresponding modes both show support in the shear layer as well as the far wake. This, along with the fact that neither appears in POD analysis, suggests that these modes may be related to the interaction of the shear layer and wake. Measurements taken with a probe verify that the nonharmonic shear layer frequency is indeed observed in the flow.

Motivated by the dominance of the fundamental wake frequency, we investigate the effect of forcing the flow at a nearby frequency of $St = 0.36$. ZNMF actuation at this frequency is very effective in reducing the extent of the separation bubble. The resulting Koopman spectrum is dominated by harmonic peaks only. However, the corresponding modes resemble the nonharmonic (interaction) modes of the unactuated flow, with support in the shear layer leading into the wake. This suggests that the effectiveness of this control strategy may be tied to its enhancing the interaction modes.

Future work will focus on a continued use of Koopman spectral analysis as a complement to traditional spectral techniques. An obvious parameter of interest is the optimal forcing frequency. A coarse, wide-ranging sweep of the parameter space will be conducted in an effort to determine whether or not forcing at higher wake superharmonics (or even subharmonics) is effective. A finer sweep will also be done, in which small perturbations about the the wake frequency will be tested. In these studies, we will look to identify patterns in the nature of the Koopman spectra and modes. Commonalities that distinguish effective control strategies may lead to insight into the physical mechanisms that drive the flow.

Acknowledgements

We would like to thank the Air Force Office of Scientific Research (grant FA9550-09-1-0257) and Dr. Doug Smith for their support of this work. We would also like to acknowledge many insightful conversations with John Griffin, Kevin Chen, and Mark Luchtenberg.

References

- ¹Tian, Y., Cattafesta III, L. N., and Mittal, R., "Adaptive control of separated flow," AIAA Paper 2006-1401, Jan. 2006.
- ²Seifert, A., Darabi, A., and Wagnanski, I., "Delay of airfoil stall by periodic excitation," *J. Aircraft*, Vol. 33, No. 4, July 1996, pp. 691–698.
- ³Mittal, R., Kotapati, R. B., and Cattafesta III, L. N., "Numerical study of resonant interactions and flow control in a canonical separated flow," AIAA Paper 2005-1261, Jan. 2005.
- ⁴Bar-Sever, A., "Separation Control on an Airfoil by Periodic Excitation," *AIAA J.*, Vol. 27, No. 6, June 1989, pp. 820–821.
- ⁵Seifert, A., Bachar, T., Koss, D., Shepshelovich, M., and Wagnanski, I., "Oscillatory Blowing - A Tool to Delay Boundary-Layer Separation," *AIAA J.*, Vol. 31, No. 11, Nov. 1993, pp. 2052–2060.
- ⁶Ravindran, S. S., "Active Control of Flow Separation Over an Airfoil," Tech. rep., NASA, 1999.
- ⁷Wagnanski, I., "Some New Observations Affecting the Control of Separation by Periodic Forcing," AIAA Paper 2000-2314, jun 2000.
- ⁸Margalit, S., Greenblatt, D., Seifert, A., and Wagnanski, I., "Active Flow Control of a Delta Wing at High Active Flow Control of a Delta Wing at High Incidence Using Segmented Piezoelectric Actuators," AIAA Paper 2002-3270, June 2002.
- ⁹Darabi, A. and Wagnanski, I., "On the Transient Process of Flow Reattachment by External Excitation," AIAA Paper 2002-3163, June 2002.
- ¹⁰Funk, R. and Parekh, D., "Transient Separation Control using Pulse Combustion Actuation," AIAA Paper 2002-3166, June 2002.

- ¹¹Seifert, A. and Pack, L., "Oscillatory control of separation at high Reynolds numbers," *AIAA J.*, Vol. 37, No. 9, Sept. 1999, pp. 1062–1071.
- ¹²Greenblatt, D. and Wygnanski, I., "Parameters Affecting Dynamic Stall Control by Oscillatory Excitation," AIAA Paper 1999-3121, June 1999.
- ¹³Pack, L., Schaeffler, N., Yao, C., and Seifert, A., "Active Control of Flow Separation from the Slat Shoulder of a Supercritical Airfoil," AIAA Paper 2002-3156, June 2002.
- ¹⁴Pack, L. and Seifert, A., "Dynamics of Active Separation Control at High Reynolds Numbers," AIAA Paper 2000-0409, Jan. 2000.
- ¹⁵Gilarranz, J. L. and Rediniotis, O. K., "Compact, High-Power Synthetic Jet Actuators for Flow Separation Control," AIAA Paper 2001-0737, Jan. 2001.
- ¹⁶Amitay, M., Smith, D., Kibens, V., Rarekh, D., and A., G., "Aerodynamic Flow Control over an Unconventional Airfoil Using Synthetic Jet Actuators," *AIAA J.*, Vol. 39, No. 3, March 2001, pp. 361–370.
- ¹⁷He, Y. Y., W, C. A., and A, P. D., "Parametric and Dynamic Modeling for Synthetic Jet Control of a Post-Stall Airfoil," AIAA Paper 2001-0733, Jan. 2001.
- ¹⁸Miranda, S., Telionis, D., and Zeiger, M., "Flow Control of a Sharp Edged Airfoil," AIAA Paper 2001-0119, Jan. 2001.
- ¹⁹Chen, F. J. and Beeler, G. B., "Virtual Shaping of a Two-Dimensional NACA 0015 Airfoil Using Synthetic Jet Actuator," AIAA Paper 2002-3273, June 2002.
- ²⁰Wu, J., Lu, X., Denny, A., Fan, M., and Wu, J., "Post-stall flow control on an airfoil by local unsteady forcing," *J. Fluid Mech.*, Vol. 371, Sept. 1998, pp. 21–58.
- ²¹Kotapati, R. B., Mittal, R., Marxen, O., Ham, F., and You, D., "Numerical simulations of synthetic jet based separation control in a canonical separated flow," AIAA Paper 2007-1308, Jan. 2007.
- ²²Cullen, L., Nishri, B., Greenblatt, D., and Wygnanski, I., "The Effect of Curvature on Boundary Layers Subjected to Strong Adverse Pressure Gradients," AIAA Paper 2002-0578, Jan. 2002.
- ²³Greenblatt, D. and Wygnanski, I., "Effect of Leading-Edge Curvature and Slot Geometry on Dynamic Stall Control," AIAA Paper 2002-3271, June 2002.
- ²⁴Greenblatt, D. and Wygnanski, I., "Effect of leading-edge curvature on airfoil separation control," *J. Aircraft*, Vol. 40, No. 3, May 2003, pp. 473–481.
- ²⁵Aram, E., Mittal, R., Griffin, J., and Cattafesta, L., "Towards Effective ZNMF Jet Based Control of a Canonical Separated Flow," AIAA Paper 2010-4705, June 2010.
- ²⁶Raju, R., Aram, E., Mittal, R., and Cattafesta, L., "Simple Models of Zero-Net Mass-Flux Jets for Flow Control Simulations," *Int. J. Flow Contr.*, Vol. 1, No. 3, 2009, pp. 179–198.
- ²⁷Kotapati, R. B., Mittal, R., and Cattafesta, III, L. N., "Numerical study of a transitional synthetic jet in quiescent external flow," *J. Fluid Mech.*, Vol. 581, June 2007, pp. 287–321.
- ²⁸Mittal, R., Dong, H., Bozkurttas, M., Najjar, F. M., Vargas, A., and von Loebbecke, A., "A versatile sharp interface immersed boundary method for incompressible flows with complex boundaries," *J. Comput. Phys.*, Vol. 227, No. 10, May 2008, pp. 4825–4852.
- ²⁹Rowley, C. W., Mezic, I., Bagheri, S., Schlatter, P., and Henningson, D. S., "Spectral analysis of nonlinear flows," *J. Fluid Mech.*, Vol. 641, Dec. 2009, pp. 115–127.
- ³⁰Schmid, P. J., "Dynamic mode decomposition of numerical and experimental data," *J. Fluid Mech.*, Vol. 656, 2010, pp. 5–28.
- ³¹Noack, B., Afanasiev, K., Morzynski, M., Tadmor, G., and Thiele, F., "A hierarchy of low-dimensional models for the transient and post-transient cylinder wake," *J. Fluid Mech.*, Vol. 497, Dec. 2003, pp. 335–363.